Monthly Notices of the ROYAL ASTRONOMICAL SOCIETY

MNRAS **503,** 5984–5996 (2021) doi:10.1093/mnras/stab791
Advance Access publication 2021 March 18

WISDOM project – VII. Molecular gas measurement of the supermassive black hole mass in the elliptical galaxy NGC 7052

Mark D. Smith [1]★ Martin Bureau,[1,2] Timothy A. Davis [3] Michele Cappellari [1] Lijie Liu,[1] Kyoko Onishi [4] Satoru Iguchi [5,6] Eve V. North [3] Marc Sarzi[7] and Thomas G. Williams [3,8]

[1]*Sub-department of Astrophysics, Department of Physics, University of Oxford, Denys Wilkinson Building, Keble Road, Oxford OX1 3RH, UK*
[2]*Yonsei Frontier Lab and Department of Astronomy, Yonsei University, 50 Yonsei-ro, Seodaemun-gu, Seoul 03722, Republic of Korea*
[3]*School of Physics & Astronomy, Cardiff University, Queens Buildings, The Parade, Cardiff CF24 3AA, UK*
[4]*Department of Space, Earth and Environment, Chalmers University of Technology, Onsala Observatory, SE-439 92 Onsala, Sweden*
[5]*Department of Astronomical Science, SOKENDAI (The Graduate University of Advanced Studies), Mitaka, Tokyo 181-8588, Japan*
[6]*National Astronomical Observatory of Japan, National Institutes of Natural Sciences, Mitaka, Tokyo 181-8588, Japan*
[7]*Armagh Observatory and Planetarium, College Hill, Armagh BT61 DG, UK*
[8]*Max Planck Institut für Astronomie, Königstuhl 17, D-69117 Heidelberg, Germany*

Accepted 2021 March 15. Received 2021 March 15; in original form 2020 April 14

ABSTRACT

Supermassive black hole (SMBH) masses can be measured by resolving the dynamical influences of the SMBHs on tracers of the central potentials. Modern long-baseline interferometers have enabled the use of molecular gas as such a tracer. We present here Atacama Large Millimeter/submillimeter Array observations of the elliptical galaxy NGC 7052 at 0.″11 (37 pc) resolution in the ^{12}CO(2-1) line and 1.3 mm continuum emission. This resolution is sufficient to resolve the region in which the potential is dominated by the SMBH. We forward model these observations, using a multi-Gaussian expansion of a *Hubble Space Telescope* F814W image and a spatially constant mass-to-light ratio to model the stellar mass distribution. We infer an SMBH mass of $2.5 \pm 0.3 \times 10^9\,\mathrm{M}_\odot$ and a stellar *I*-band mass-to-light ratio of $4.6 \pm 0.2\,\mathrm{M}_\odot/\mathrm{L}_{\odot,\mathrm{I}}$ (3σ confidence intervals). This SMBH mass is significantly larger than that derived using ionized gas kinematics, which however appears significantly more kinematically disturbed than the molecular gas. We also show that a central molecular gas deficit is likely to be the result of tidal disruption of molecular gas clouds due to the strong gradient in the central gravitational potential.

Key words: galaxies: elliptical and lenticular, cD – galaxies: individual: NGC 7052 – galaxies: ISM – galaxies: kinematics and dynamics – galaxies: nuclei.

1 INTRODUCTION

Supermassive black holes (SMBHs) are characterized by just a few properties: their masses, spins and charges. An SMBH mass can be measured by spatially and/or temporally resolving a dynamical tracer of the central potential, most commonly stars or ionized gas (see Kormendy & Richstone 1995 for a review contrasting these two methods), or more rarely masers (e.g. Greenhill et al. 1995; Miyoshi et al. 1995). The last three decades of studies have demonstrated that SMBH masses correlate tightly with a wide variety of properties of their host galaxies, including the stellar velocity dispersion (e.g. Ferrarese & Merritt 2000; Gebhardt et al. 2000), bulge mass and/or luminosity (e.g. Kormendy & Richstone 1995; Magorrian et al. 1998), total luminosity (e.g. Kormendy & Gebhardt 2001) and Sérsic index (e.g. Graham et al. 2001). These correlations are sufficiently tight to imply (potentially self-regulating) co-evolutionary processes. That the tightest correlations are found with the properties of classical (merger-formed) bulges (e.g. Gültekin et al. 2009; Beifiori et al. 2012; Saglia et al. 2016; van den Bosch 2016) suggests that mergers may be important (either via the SMBHs themselves merging or by the disrupted potential leading to enhanced accretion on to a central SMBH; e.g. Sanders et al. 1988; Hernquist 1989; Di Matteo, Springel & Hernquist 2005). However, the potential importance of secular accretion on to an SMBH, coupled with galactic evolution at larger spatial scales via active galactic nucleus (AGN) feedback, cannot be discounted. Simulations indicate that such feedback is vital for replicating observed properties on large scales (e.g. Benson et al. 2003; McNamara & Nulsen 2007). Nevertheless, the relative importance of these processes remains disputed (e.g. Kormendy & Ho 2013; Simmons, Smethurst & Lintott 2017; Krajnović, Cappellari & McDermid 2018).

Molecular gas emission has proved to be a suitable tracer of SMBH potentials (e.g. Davis et al. 2013b) for galaxies across the Hubble sequence, including those hosting AGN. Our millimetre-Wave Interferometric Survey of Dark Object Masses (WISDOM) exploits the high angular resolution available from modern interferometers to spatially resolve CO emission on SMBH-dominated scales. In previous papers in this sequence, we have presented new SMBH measurements (Davis et al. 2017, 2018; Onishi et al. 2017; North et al. 2019; Smith et al. 2019), explored a correlation between CO line width and SMBH mass (Smith et al. 2021), and studied the properties

★ E-mail: mark.smith@jesus.ox.ac.uk

© 2021 The Author(s).
Published by Oxford University Press on behalf of Royal Astronomical Society. This is an Open Access article distributed under the terms of the Creative Commons Attribution License (http://creativecommons.org/licenses/by/4.0/), which permits unrestricted reuse, distribution, and reproduction in any medium, provided the original work is properly cited.

Downloaded from https://academic.oup.com/mnras/article/503/4/5984/6177668 by Cardiff University user on 22 July 2021

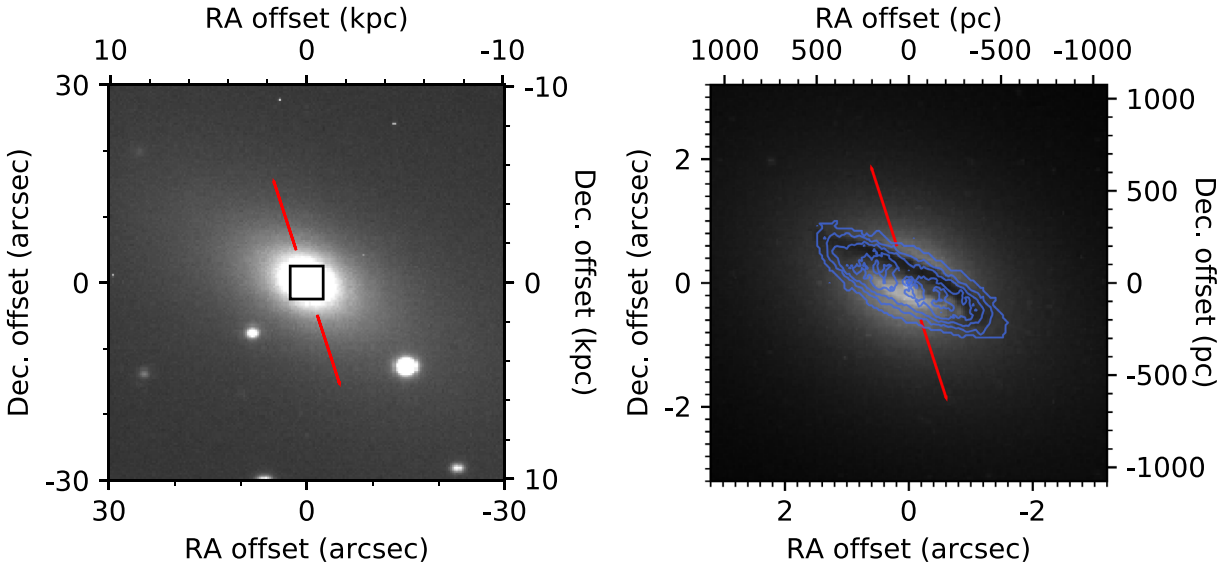

Figure 1. Left panel: Jakobus Kapteyn Telescope *V*-band image of NGC 7052 (greyscale), showing the large-scale morphology of NGC 7052. The black central box is the area shown in the right panel. Right panel: Unsharp-masked *HST* WFPC2/PC F814W image of NGC 7052 (greyscale; van der Marel & van den Bosch 1998), showing the central dust disc. Overlaid are the H_2 surface density contours (blue) inferred from our ALMA observations, assuming a CO(2-1)/CO(1-0) line ratio of unity and $\alpha_{CO} = 4.3\,M_\odot\,(K\,km\,s^{-1})^{-1}\,pc^{-2}$. The contours are from the level at which the noise was clipped, $15\,M_\odot\,pc^{-2}$, and then at 4000, 8000, 12 000, and 16 000 $M_\odot\,pc^{-2}$. Spatial offsets are relative to the 1.3 mm continuum source position listed in Table 2. The red lines in each panel indicate the 6 cm radio emission axis (Condon, Frayer & Broderick 1991).

of the cold molecular interstellar medium at very high resolution in local galaxies (Liu et al. 2021). In parallel, other groups have used this technique to measure SMBH masses in various other galaxies (e.g. Barth et al. 2016a, b; Boizelle et al. 2019; Nagai et al. 2019; Thater et al. 2020). Notably, using this method, robust constraints have even been placed on a few SMBH masses in dwarf galaxies (Davis et al. 2020; Nguyen et al. 2020).

In this paper, we use new high-resolution observations of the galaxy NGC 7052 to measure its central SMBH mass. In Section 2, we describe the properties of our target galaxy. Section 3 describes the Atacama Large Millimeter/submillimeter Array (ALMA) observations, their calibration and imaging. The dynamical model we fit to our observations is described in Section 4, and we discuss our results in Section 5. We conclude briefly in Section 6. Throughout this paper, velocities are given in the radio convention.

2 NGC 7052

NGC 7052 is an isolated elliptical radio galaxy (Fig. 1, left panel) in the Vulpecula constellation, located at $21^h18^m33^s, +26°26'49''$. Its total stellar mass is $5.6 \times 10^{11}\,M_\odot$ (Pandya et al. 2017), among the most massive galaxies in the local universe, and it is a member of the MASSIVE sample of such galaxies (Ma et al. 2014). The near-infrared effective (i.e. half-light) radius (R_e) is 14.″7 (Ma et al. 2014). The galaxy is kinematically classified as a slow-rotator according to the criterion of Emsellem et al. (2011), based on the projected stellar angular momentum λ_e (spin parameter) averaged within one effective radius ($\lambda_e = 0.15$; Veale et al. 2017). Throughout this paper, we adopt the distance used in the MASSIVE survey, $D = 69.3$ Mpc. This distance is calculated from the observed recession velocity and the flow model of Mould et al. (2000) assuming a current Hubble constant $H_0 = 70\,km\,s^{-1}\,Mpc^{-1}$. At this distance, 1 arcsec corresponds to 336 pc.

Radio jets have been mapped in NGC 7052 on arcminute scales at 1.5 and 5 GHz using the Very Large Array (VLA; Parma et al. 1986) and Westerbork Synthesis Radio Telescope (WSRT; Fanti et al. 1977), respectively. The radially declining profile of this emission indicates the galaxy is a Fanaroff-Riley Class I source (FR-I; Capetti et al. 2000, 2002).

X-ray emission from the galaxy has been detected and extensively studied (e.g. Donato, Sambruna & Gliozzi 2004; Mulchaey & Jeltema 2010; Goulding et al. 2016). Memola et al. (2009) used *Chandra* observations to separate the contribution of the AGN from that of the spatially unresolved X-ray binaries, determining an AGN X-ray luminosity of $L_{AGN,X} \approx 10^{33}$ W.

Optical images from the *Hubble Space Telescope* (*HST*) reveal that the centre of NGC 7052 harbours a prominent nuclear dust disc with a dust mass of $\approx 10^4\,M_\odot$ (Nieto et al. 1990), shown here in extinction in Fig. 1 (right-hand panel). This dust disc has a semimajor (-minor) axis of 1.″94 (0.″67); assuming the dust disc has no intrinsic thickness yields an inclination estimate of $70° \pm 2°$ (van der Marel & van den Bosch 1998). Although the dust disc is very prominent to the north-west of the nucleus, it does not appear to significantly obscure the nucleus itself (Capetti et al. 2000). It is not orthogonal to the radio emission (Capetti & Celotti 1999).

Despite being an early-type galaxy, NGC 7052 hosts a significant molecular gas reservoir with a total mass of $2.3 \times 10^9\,M_\odot$ (Wang, Kenney & Ishizuki 1992, corrected to $\alpha_{CO} = 4.3\,M_\odot\,(K\,km\,s^{-1})^{-1}\,pc^{-2}$). Warm gas makes up only a very small proportion of the galaxy's mass budget, totalling only $4 \times 10^3\,M_\odot$ (estimated from the Hβ luminosity) over the central 1.7 kpc radius (Pandya et al. 2017).

HST Faint Object Spectrograph (FOS) observations of the Hα and [N II] emission lines along the major axis were modelled by van der Marel & van den Bosch (1998) to determine a central SMBH mass of $M_{BH} = 3.9^{+2.7}_{-1.5} \times 10^8\,M_\odot$ (corrected to our adopted distance), robustly excluding models without a central SMBH. However, the ionized gas kinematics in the centre of the galaxy are dominated by turbulent motions (exceeding 400 km s^{-1}), the potential dynamical support of which were neglected by van der Marel & van den Bosch (1998). This likely leads to an underestimated SMBH mass, as seen

Downloaded from https://academic.oup.com/mnras/article/503/4/5984/6177668 by Cardiff University user on 22 July 2021

Table 1. Properties of the four observing tracks.

Track	Date	Array	Baseline range	On-source time	Calibration
uid_A002_Xc39302_X5d57	2017 August 21	7-m	9 m–45 m	32 min	Pipeline
uid_A002_Xd44a99_X974	2018 October 31	12-m	15 m–1.4 km	5 min	Pipeline
uid_A002_Xdfcc3f_X1c7a	2019 August 8	12-m	40 m–5.9 km	21 min	Manual
uid_A002_Xdfdbea_X598	2019 August 9	12-m	40 m–5.9 km	21 min	Pipeline; antenna DA45 flagged

for example in Centaurus A (Häring-Neumayer et al. 2006). Cold molecular gas generally exhibits smaller velocity dispersions, allowing an independent, and likely more reliable, dynamical SMBH mass measurement. While the most precise SMBH mass measurements so far have been achieved by tracing maser emission very close to the SMBHs with very long baseline interferometry (VLBI; e.g. Miyoshi et al. 1995; Kuo et al. 2011; Gao et al. 2017), no 22 GHz maser emission was detected in NGC 7052 with the Effelsberg 100-m telescope (Braatz, Wilson & Henkel 1996), leaving cold molecular gas the most promising option.

The sphere of influence of the SMBH, the approximate physical scale at which the SMBH dominates the gravitational potential, is given by $R_{\rm SoI} \equiv GM_{\rm BH}/\sigma_{\rm e}^2$, where G is the gravitational constant, $M_{\rm BH}$ the SMBH mass and $\sigma_{\rm e}$ the stellar velocity dispersion averaged within 1 $R_{\rm e}$. Using the distance-corrected SMBH mass from van der Marel & van den Bosch (1998) and $\sigma_{\rm e} = 266 \pm 13$ km s^{-1}(Gültekin et al. 2009), we estimate $R_{\rm SoI} = 24 \pm 13$ pc ($0\farcs07 \pm 0\farcs04$).

3 ALMA OBSERVATIONS

NGC 7052 was observed with the ALMA 12-m array as part of the WISDOM project 2018.1.00397.S. An extended ALMA configuration was used to provide baselines of 40 m–5.9 km, in two tracks on 8th and 9th August 2018, each on-source for 21 minutes. The former track failed the online ALMA quality assessment check (known as QA0) due to large residuals in the phase calibration, and therefore the second track was taken. Manual calibration was performed on the first track by the United Kingdom ALMA Regional Centre, recovering much of the data for further use. The second track was automatically calibrated by the ALMA pipeline, and one antenna (DA45) was subsequently manually flagged due to an amplitude error.

To better sample the *uv* plane and thus recover any large-scale structure, additional observations were taken with a compact ALMA configuration and with the 7-m Atacama Compact Array (ACA). The additional 12-m track on 31st October 2018 covered baselines 15 m–1.4 km and was on-source for 5 minutes. The ACA track was obtained as part of programme 2016.2.00046.S, was observed on 21st August 2019, covered baselines 9 – 45 m, and was on-source for 32 minutes. Both of these tracks were automatically calibrated by the ALMA pipeline.

The properties of these four observing tracks are listed in Table 1. Combining all four tracks together yields continuous baseline coverage from 9 m to 5.9 km, corresponding to sensitivity to angular scales from $0\farcs06$ to 36 arcsec. The dust disc visible in optical images of NGC 7052 has a major- (minor-)axis diameter of ≈4 arcsec (≈1 arcsec). Assuming the CO is co-spatial with the dust disc, we therefore expect to recover all the emitted flux.

Two spectral set-ups were used. For all 12-m array observations, a 1.875 GHz bandwidth spectral window with a channel width of ≈1 MHz was placed over the ^{12}CO(2-1) emission line. At this frequency, this corresponds to a ≈2400 km s^{-1} velocity range and ≈1 km s^{-1} channels. The ACA observations used a slightly different receiver configuration, with one 2 GHz (≈2600 km s^{-1}) bandwidth spectral window and 500 kHz (≈0.7 km s^{-1}) channels. In both cases, the remaining three 2 GHz bandwidth spectral windows were placed to detect continuum emission.

Table 2. Parameters of the continuum image and the detected 1.3 mm continuum source.

Image property	Value
Image size (pix)	512 × 512
Image size (arcsec)	10.24 × 10.24
Image size (pc)	3440 × 3440
Pixel scale (arcsec pix^{-1})	0.02
Pixel scale (pc pix^{-1})	6.72
1σ sensitivity (μJy beam^{-1})	80
Synthesized beam (arcsec)	0.12 × 0.09
Synthesized beam (pc)	38 × 27
Source property	**Value**
Right ascension	$21^{\rm h}18^{\rm m}33\fs0433 \pm 0\fs0001$
Declination	$+26°26'49\farcs242 \pm 0\farcs003$
Integrated flux (mJy)	22.3 ± 1.5
Deconvolved size (arcsec)	$(0.07 \pm 0.02) \times (0.05 \pm 0.03)$
Deconvolved size (pc)	$(22 \pm 6) \times (16 \pm 9)$

3.1 Continuum images

The calibrated observations were concatenated (with default weighting and the `concat` task) using the `Common Astronomy Software Applications (CASA)` package (McMullin et al. 2007), and an image of the 1.3 mm continuum was created using the `CASA` task `tclean` in multifrequency synthesis mode. The continuum spectral windows and line-free channels of the line spectral window were used. The image was made using Briggs weighting with a robust parameter of 0, balancing angular resolution and sensitivity. An approximately point-like continuum source was detected and fit with a 2D Gaussian using the `CASA` task `imfit`. The properties of this continuum image and of the detected continuum source are listed in Table 2.

3.2 Line images

A linear fit to the continuum spectral windows and line-free channels of the line spectral window was subtracted from the *uv*-plane data using the `CASA` task `uvcontsub`. The continuum-subtracted data were then concatenated, imaged and cleaned using the 'cube' mode of the `tclean` task and adopting Briggs weighting with robust = 0. The properties of the resulting image cube are listed in Table 3.

The molecular gas distribution, mean line-of-sight velocity field, velocity dispersion field, and kinematic major axis position–velocity diagram (PVD) are shown in Fig. 2. These were made with the masked-moments method (Dame 2011), whereby the cube is first convolved spatially by the beam and Hanning-smoothed spectrally,

Downloaded from https://academic.oup.com/mnras/article/503/4/5984/6177668 by Cardiff University user on 22 July 2021

Table 3. Parameters of the CO line cube.

Image property	Value
Image size (pix)	512×512
Image size (arcsec)	10.24×10.24
Image size (pc)	3440×3440
Pixel scale (arcsec pix^{-1})	0.02
Pixel scale (pc pix^{-1})	6.72
Velocity range (km s^{-1})	$4035 - 5235$
Channel width (km s^{-1})	15
1σ sensitivity (mJy beam^{-1})	0.5
1σ sensitivity (M$_\odot$ pc^{-2})	15
Synthesized beam (arcsec)	0.13×0.10
Synthesized beam (pc)	41×30

pixels that exceed a noise threshold are included in a mask, and this mask is then applied to the original cube. This method selects only areas of structured emission in the original cube and excludes regions with no significant emission, thus producing improved moment maps. The spectrally integrated intensity map is then converted into molecular gas surface densities by appropriately modifying equation (3) of Bolatto, Wolfire & Leroy (2013), and adopting a CO(2-1)/CO(1-0) line ratio of unity and $\alpha_{\rm CO} = 4.3\,{\rm M}_\odot$ (K km s^{-1})$^{-1}$ pc^{-2}.

The CO gas in NGC 7052 is distributed in a regularly rotating disc, coincident with the dust disc (Fig. 1, right-hand panel). The total molecular gas mass derived from our data is $1.8 \times 10^9\,{\rm M}_\odot$. This is very similar to the single-dish measurement of Wang et al. (1992), and likely fully consistent once the systematic uncertainties on the absolute flux calibrations of ALMA and the Nobeyama 45-m telescope are considered, further evidence that we have not resolved out significant flux. The CO surface density peaks along the major axis at $\approx$0.″5 on either side of the centre, rapidly decreasing toward the nucleus and more slowly outward. In the very centre of the galaxy is a small hole, where the gas surface density is below our sensitivity limit of $15\,{\rm M}_\odot$ pc^{-2}.

In principle, such a hole could be an artefact caused by projecting the cube on to an image. Indeed, the mask could exclude gas close to the SMBH where the line-of-sight velocity distribution becomes very broad, causing emission to be spread over many channels (and therefore fall below our sensitivity limit in any given channel). However, we have checked that a manually defined mask including all channels within the hole does not recover any more emission. Another possibility is that a few channels showing absorption against the continuum source contribute negative flux in this region (once continuum subtracted), reducing the sum. There is however no evidence of such absorption features in the spectra within the hole. To further exclude the possibility that erroneous continuum-subtraction has created the hole, we made a second data cube from the observations without first subtracting the continuum. The hole was still visible in this cube, the continuum source not being sufficiently extended to fill the void. Having excluded these two explanations, we conclude that the hole is genuine and astrophysical in origin. We discuss it further in Section 5.5.

Such holes appear to be common in the galaxies studied in the WISDOM survey. Typically, they have spatial extents similar to those of the SMBH spheres-of-influence, occasionally preventing the detection of the central Keplerian rotation (e.g. Davis et al. 2018; Smith et al. 2019). In such cases we have nevertheless been able to measure the SMBH masses, as the SMBH's presence still enhances the gas velocities above those expected from the stars alone.

The kinematic major axis PVD (Fig. 2, bottom-right panel) shows a rotation curve that rises towards the centre with decreasing radius at radii $r < 0.''5$, as would be expected from Keplerian rotation around a compact mass. The signature is most prominent on the north-east side of the galaxy (positive velocities), albeit only in the faintest contour, while it is only marginally visible on the south-west side (negative velocities), due to the slight asymmetry of the CO disc. Additional evidence for the enhanced velocities due to the presence of a central mass concentration is given by the shape of the PVD envelope. The gas remains at high velocities to very small radii ($\approx$250 km s^{-1} at 0.″2 or 70 pc), before falling very steeply. In the absence of a central mass concentration, a shallower central decline would be expected.

The velocity dispersion map (Fig. 2, bottom-left panel) indicates that the gas at the edge of the disc is dynamically cold ($\sigma_{\rm gas} < 30$ km s^{-1}). As the gas density increases, the dispersion also increases, but in the centre of the disc it is likely that the line-of-sight velocity dispersion is dominated by (beam) smearing of closely spaced isovelocity contours. This suggests that the molecular gas remains dynamically cold throughout the disc, in contrast to the strong gradients observed in ionized gas (van den Bosch & van der Marel 1995). We will further test this conclusion using our dynamical modelling in Section 4.

4 DYNAMICAL MODELLING

Dynamical modelling of NGC 7052 was carried out using the same methods as extensively discussed in previous works of this series (particularly Davis et al. 2017 and Smith et al. 2019), so we provide only an outline of our procedures here, before discussing in greater detail features of the model unique to this case.

Simulated data cubes were constructed from dynamical models of the molecular gas disc in NGC 7052 using the `Integrated Development Language (IDL)` version of the `Kinematic Molecular Simulation (KinMS)` tool[1] (Davis et al. 2013a). These were fit to the observed data cube using a Markov-chain Monte Carlo (MCMC) method with a custom Gibbs sampler (`KinMS_mcmc`[2]). `KinMS` generates a set of particles at positions replicating a specified surface brightness profile, it assigns to each particle the velocity expected at its radius from a specified circular velocity curve (although every particle is also assigned an additional random velocity, depending on the velocity dispersion selected by the user, that is not taken into account dynamically), it projects these velocities along the line of sight (according to the specified galaxy viewing angles), and it places the particle into a data cube. This cube is then convolved spatially by the synthesized beam to replicate instrumental effects.

The circular velocity at every radius is calculated (using the `IDL` procedure `MGE_CIRCULAR_VELOCITY`[3]) from the SMBH mass and a model of the stellar mass distribution, parametrized by a multi-Gaussian expansion (MGE; Emsellem, Monnet & Bacon 1994; Cappellari 2002) of an *HST* image and a stellar mass-to-light ratio M/L. This stellar contribution is explained in further detail in Section 4.1, listed in Table 4, and shown in Fig. 3.

In addition to these three dynamical parameters (SMBH mass, stellar mass-to-light, ratio and gas velocity dispersion), and two parameters specifying the disc orientation relative to the observer (inclination and position angle), we also allow the model to vary

[1] https://github.com/TimothyADavis/KinMS
[2] https://github.com/TimothyADavis/KinMS_mcmc
[3] http://purl.org/cappellari/software

Downloaded from https://academic.oup.com/mnras/article/503/4/5984/6177668 by Cardiff University user on 22 July 2021

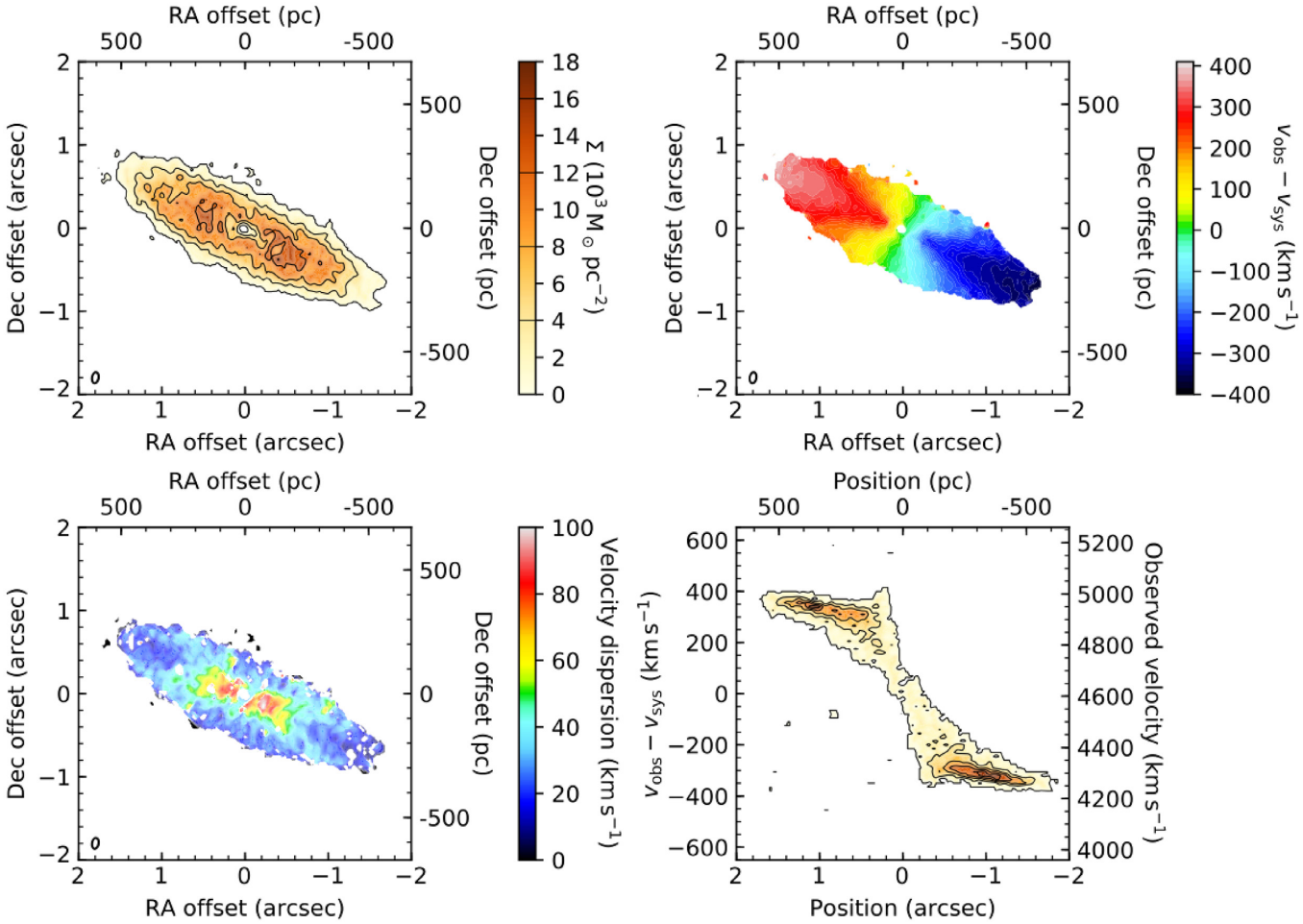

Figure 2. Moment maps of the ^{12}CO(2-1) emission in NGC 7052 centred on the compact continuum source. Top-left: Molecular gas surface density (orange scale and black contours), assuming a CO(2-1)/CO(1-0) line ratio of unity and $\alpha_{CO} = 4.3\,M_\odot\,(K\,km\,s^{-1})^{-1}\,pc^{-2}$. Black contours are from the level at which the noise was clipped, $15\,M_\odot\,pc^{-2}$, and then at 4000, 8000, 12 000 and 16 000 $M_\odot\,pc^{-2}$. Top-right: Mean line-of-sight velocity. Bottom-left: Line-of-sight velocity dispersion. Bottom-right: Kinematic major axis position–velocity diagram (PVD; orange scale and black contours). In both right panels, v_{obs} is the observed line-of-sight velocity and $v_{sys} = 4610\,km\,s^{-1}$ is the galaxy systemic velocity in the radio convention. The maps show the synthesized beam in their bottom-left corners.

four 'nuisance' parameters. The kinematic centre of the galaxy can have small spatial and velocity offsets with respect to the location of the aforementioned continuum source and the galaxy systemic velocity, and we let the surface brightness function have an arbitrary overall scaling.

4.1 Stellar potential

The stellar potential is determined from a *HST* Wide Field Planetary Camera 2 (WFPC2) Planetary Camera (PC) F814W image originally presented in van der Marel & van den Bosch (1998). We fit the entire PC image. We adopt the point spread function appropriate for WFPC2/PC F814W, given in table 3 of Cappellari et al. (2002). To minimize the impact of extinction from the dust disc on our MGE model of the F814W image, we mask the north-western side of the dust disc, which appears to be in the foreground. We nevertheless include the central 9×9 pixels to robustly constrain the stellar light in the galactic centre.

The MGE model consists of the deconvolved central intensity (I'), width (σ) and apparent flattening (q') of a sequence of 2D Gaussians that accurately replicate the observed (i.e. 2D, projected) light distribution. We convert these components to physical units (*I*-band solar luminosity surface densities $L_{\odot,I}\,pc^{-2}$) adopting a zero-point of 20.84 mag (Holtzman et al. 1995) and an *I*-band Solar absolute magnitude of 4.12 (Willmer 2018), both in the Vega system. These components are listed in Table 4 and the fit is shown in Fig. 3. The dust disc is evident in the distortions to the (otherwise elliptical) isophotes.

Table 4. Spatially deconvolved 2D MGE components of the model of our *HST* WFPC2/PC F814W image of NGC 7052.

$\log_{10}\left(\frac{I'_j}{L_{\odot,I}\,pc^{-2}}\right)$	$\log_{10}\left(\frac{\sigma_j}{arcsec}\right)$	q'_j
(1)	(2)	(3)
4.49	−1.76	0.73
3.93	−0.23	0.77
3.67	0.14	0.69
3.56	0.60	0.71

Note. The table lists the central surface brightness (column 1), width (column 2), and axial ratio (column 3) of each deconvolved Gaussian component.

Downloaded from https://academic.oup.com/mnras/article/503/4/5984/6177668 by Cardiff University user on 22 July 2021

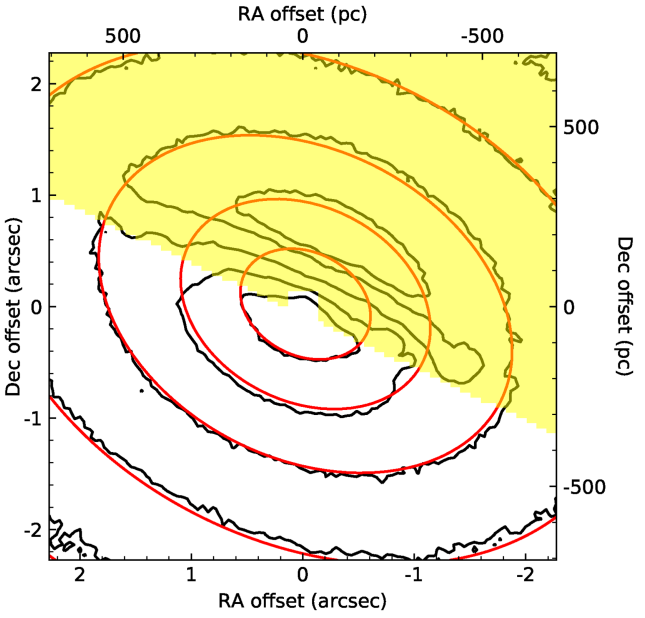

Figure 3. *HST* WFPC2/PC F814W image of NGC 7052 (black contours), overlaid with our MGE model (red contours). The north-western side of the image is masked (yellow) to exclude the foreground dust disc, but we retain the central 9 × 9 pixels.

The MGE components describing the stellar light distribution can be converted into a mass distribution by multiplying the luminosity surface density of each Gaussian by the mass-to-light ratio. We assume this mass-to-light ratio to be radially constant, though we discuss this assumption further in Section 5.1. Assuming an inclination, the projected stellar light (or mass) distribution can be analytically deprojected into a 3D distribution, and the circular velocity resulting from this distribution can be calculated.

We will ultimately find that the stellar mass contribution to the potential within the central few resolution elements is negligible, and thus does not affect the best-fitting SMBH mass. This is corroborated by the spatially resolved central Keplerian rotation curve, indicating that the central potential is dominated by a compact mass. In consequence, any extinction of the dust disc in the background of the south-eastern side of the galaxy does not significantly bias the inferred SMBH mass.

4.2 Molecular gas geometry

In previous works in this series, we have commonly parametrized the molecular gas distribution using an axisymmetric exponential disc. The extremely high angular resolutions achieved with ALMA have however revealed that many objects host a central hole, that we have typically included using an additional central truncation. However, many galaxies have a molecular gas distribution which cannot be described by such a simple function. Smith et al. (2019) presented a new approach, using the `SkySampler` tool[4] to infer the spatially deconvolved projected gas distribution (once reconvolved by the synthesized beam, this distribution is equivalent to the top-left panel of Fig. 2), deproject this distribution into the disc plane under the thin disc assumption, and then calculate the associated line-of-sight velocities for the distribution as before. By construction, the model matches the observed gas distribution. The gas distribution therefore offers no constraint on the model parameters, but `SkySampler` allows us to remove a few degrees of freedom from the model.

We adopt this approach for NGC 7052. The molecular gas surface brightness distribution appears to peak at a radius of ≈0.″5, before declining toward the centre of the galaxy (and outward). Attempting a fit using an exponential disc and central truncation failed to adequately reproduce the observed gas distribution. For our final fit, we therefore instead built a `SkySampler` model of the gas distribution from the projected `CLEAN` components, thus avoiding oversmoothing our model.

4.3 Bayesian inference and priors

The MCMC fit to our data explores the posterior probability distribution of our model, given by Bayes' theorem. Assuming uniform (maximum-ignorance) priors, and that our data has a Gaussian noise distribution constant for all pixels, the posterior is then proportional to the log-likelihood ($\ln P \propto -0.5\,\chi^2$), where the chi-squared goodness-of-fit statistic is given by

$$\chi^2 \equiv \sum_i \left(\frac{\mathrm{data}_i - \mathrm{model}_i}{\sigma_i} \right)^2 = \frac{1}{\sigma^2} \sum_i (\mathrm{data}_i - \mathrm{model}_i)^2 \ , \qquad (1)$$

where the sum is performed over all the pixels within the region of the data cube that the model fits, and σ is the rms noise measured in line-free channels of the data cube.

Due to the very large number of constraints when fitting the entire 3D data cube, the ordinary assumption that the 1σ (67 per cent) confidence interval corresponds to $\Delta\chi^2 \equiv \chi^2 - \chi^2_{\mathrm{min}} = 1$ (where χ^2_{min} is the absolute χ^2 minimum across all parameters explored) yields unrealistically small formal uncertainties. We therefore rescale the standard $\Delta\chi^2$ by a factor $\sqrt{2(N-P)} \approx \sqrt{2N}$, where $N \approx 10^5$ is the number of constraints and $P = 9$ is the number of free parameters of our model. This effectively rescales the uncertainties associated with our model parameters. This approach has been used in previous works of this series (e.g. North et al. 2019; Smith et al. 2019) and other works encountering the same problem (e.g. van den Bosch & van de Ven 2009; Mitzkus, Cappellari & Walcher 2017). Smith et al. (2019) showed that this correction yields formal uncertainties that are consistent with those found by a bootstrap approach, and are thus more credible.

However, since adjacent pixels in our observations are not independent (i.e. the data are intrinsically spatially convolved by the synthesized beam, that is oversampled by our cube; see Table 3), failing to correct for pixel-to-pixel covariances would lead to underestimating the uncertainties. In previous works, we have corrected equation (1) accordingly. The disadvantage of using this correction is that we need to introduce the inverse covariance matrix (with N^2 elements) to the calculated deviations, and in consequence can only fit a relatively small region of the cube. However, this correction is negligible compared to the $\sqrt{2N}$ rescaling described above, and so we neglect it in this work. This enables us to fit the entire molecular gas disc, rather than only some smaller central region as was previously necessary.

Finally, we impose physical bounds on each parameter to ensure the chain converges in a finite time, and that it does not explore unphysical regions of parameter space. Assuming maximal ignorance, we adopt uniform priors for all parameters except M_{BH} (see Table 5). As the SMBH mass can potentially span many orders of magnitude, we adopt instead a prior that is uniform in log-space for this single parameter, thus avoiding unduly favouring large values.

[4] https://github.com/Mark-D-Smith/KinMS-skySampler

Downloaded from https://academic.oup.com/mnras/article/503/4/5984/6177668 by Cardiff University user on 22 July 2021

Table 5. Best-fitting model parameters, with associated formal uncertainties.

Parameter (1)	Priors (2)	Best fit (3)	Median (4)	1σ error (5)	3σ error (6)
Mass model:					
SMBH mass (10^9 $M_\odot$)	$10^5 \rightarrow 10^{12}$	2.61	2.54	0.11	0.31
Stellar M/L_I ($M_\odot/L_{\odot,I}$)	$1 \rightarrow 10$	4.55	4.59	0.08	0.24
Molecular gas disc:					
$2\farcs5 \times 2\farcs5$ integrated intensity (Jy km s^{-1})	$1 \rightarrow 200$	30.6	30.7	0.8	2.3
Gas velocity dispersion (km s^{-1})	$1 \rightarrow 100$	23.9	24.0	1.3	3.6
Viewing geometry:					
Inclination (°)	$60 \rightarrow 89$	74.8	74.6	0.3	0.9
Position angle (°)	$0 \rightarrow 359$	64.3	64.4	0.2	0.6
Nuisance Parameters:					
Centre RA offset (arcsec)	$-0.1 \rightarrow 0.1$	0.034	0.033	0.007	0.021
Centre Dec. offset (arcsec)	$-0.1 \rightarrow 0.1$	−0.011	−0.012	0.005	0.014
Centre velocity offset (km s^{-1})	$-75 \rightarrow 75$	-4.8	-4.6	1.9	5.4

Note. Column 1 lists the input parameters of our dynamical model of NGC 7052. Column 2 lists the range allowed for each parameter, between which we adopt a uniform prior, except for the SMBH mass for which the prior is uniform in log-space. Column 3 lists the best-fitting parameter, while column 4 lists its median after marginalizing over all other parameters. Columns 5 and 6 list the 1σ (67%) and 3σ (99.7%) confidence intervals of each parameter.

4.4 Best-fitting model

We ran our MCMC chain for 100 000 steps, discarding the first 10 000 steps as a burn-in. Our best-fitting model cube replicates the observed gas disc well. Fig. 4 shows the 2D marginalization of each pair of input parameters, and the 1D marginalization (histogram) of each parameter. As can be seen, all the 1D posteriors are approximately Gaussian, indicating the MCMC chain is well-converged. The coloured points in the 2D marginalizations indicate the log-likelihood of each model. The colour scale indicates points within $\Delta\chi^2 < \sqrt{2N}$ of the best-fitting model, with white points the most likely (the best-fitting model is also shown by a solid black line in each histogram) and blue points the least likely. Grey points are realizations with $\Delta\chi^2 > \sqrt{2N}$, and are even less likely. Slight asymmetries in the posterior, resulting from the highly nonlinear model, imply that the median of each parameter is slightly different from the best-fitting parameter. However, both are consistent within the formal uncertainties for all parameters. The elliptical coloured 'contours' also indicate that the posterior is well-sampled and well-converged.

The only significant physical covariance is the well-known one between the SMBH mass and the stellar mass-to-light ratio, equivalent to the conservation of total dynamical mass. The three offset parameters (centre right ascension, declination and velocity) are also correlated, as the gas disc is systematically distributed along a single plane in the cube. A small perturbation to one parameter will thus also change the other two to remain in this plane.

The best-fitting, median, and formal uncertainties of each model parameter are listed in Table 5. The inferred SMBH mass is $(2.5 \pm 0.3) \times 10^9\,M_\odot$ and $M/L_I = (4.6 \pm 0.2)\,M_\odot/L_{\odot,I}$, where both uncertainties are the 3σ (97 per cent) confidence level.

5 DISCUSSION

5.1 Best-fitting mass model

The quality of our best-fitting model is easy to assess from a kinematic major-axis PVD, as shown in Fig. 5, although it should be noted that our fit was performed to the entire data cube, not only to this PVD. The left panel shows a fit to the observed data cube assuming no SMBH. To attempt to account for the high velocities observed at small radii, the fit adopts a larger M/L_I, however this is clearly not a good match to the observations. The right panel shows another fit assuming an SMBH mass larger than that found in our best model. The fit attempts to compensate by reducing M/L_I, however again this yields a poor fit. The central panel clearly shows that our best model recovers the observed Keplerian rotation within the central region dominated by the SMBH, and the asymmetry of this signature on either side of the disc. Since the only non-axisymmetric feature of our model is the gas distribution, it is clear that the observed asymmetry is the result of the lack of gas to properly sample the Keplerian rise on the south-western (negative velocities) side of the disc, rather than evidence of disturbed motions.

The velocity field residuals, obtained by subtracting the model velocity field from that shown in Fig. 2, show no spatial structure that would indicate organized non-circular motions (as were found in e.g. Smith et al. 2019). In addition, the very low velocity dispersions indicate that the gas velocities are dominated by circular motion. Throughout the disc, $v/\sigma \approx 15$ (where v is the deprojected rotation velocity and σ the intrinsic velocity dispersion), indicating that the gas is rotationally supported.

In principle, the stellar mass-to-light ratio can vary across the galaxy, tracing changes of the stellar population (e.g. Davis & McDermid 2017; Davis et al. 2018). No such variation is required to adequately fit our data, but as always a sudden change in the mass-to-light ratio in the centre of the galaxy could obviate the need for an SMBH. There is no photometric evidence to support such a change, and the variation required would be unphysically large – a factor of ≈50.

5.2 Systematic uncertainties

SMBH mass uncertainties due to the inclination scale as $M_{BH} \propto 1/\sin^2 i$ (e.g. Smith et al. 2019). At low inclinations, the inclination uncertainty can dominate the SMBH mass uncertainty. At the highest inclinations, other effects become important, such as the inability to resolve non-axisymmetric structures, the disc's

Downloaded from https://academic.oup.com/mnras/article/503/4/5984/6177668 by Cardiff University user on 22 July 2021

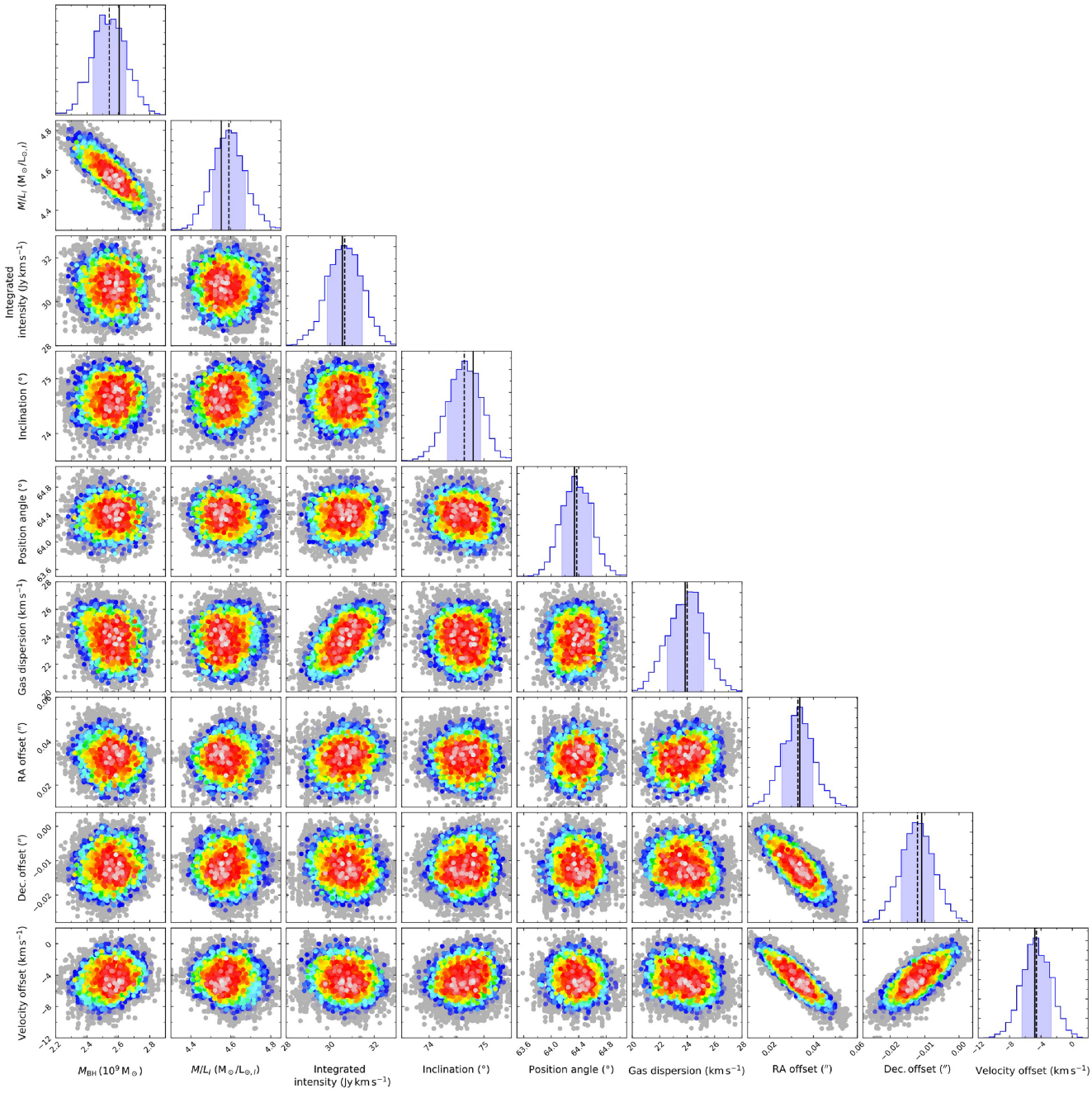

Figure 4. Corner plots showing the covariances between all model parameters, from our MCMC fit. Each point is a realization of our model, colour-coded to show the relative log-likelihood of that realization. Coloured points are within $\Delta\chi^2 < \sqrt{2N}$ relative to the best-fitting model, with white points the most likely and blue points the least likely. Grey points are realizations with $\Delta\chi^2 > \sqrt{2N}$, and are even less likely. The only significant physical covariance is between the SMBH mass and the mass-to-light ratio, that corresponds to attributing the same dynamical mass differently across the SMBH and stellar distribution. The covariances between the RA, Dec and velocity offsets correspond to moving the kinematic centre of the galaxy in three dimensions within a plane, and these offsets are much smaller than the resolution of our data. Each histogram shows the 1D marginalization of a model parameter, the black lines denoting the median (dashed) and best-fitting (solid) values. The shaded region indicates the 68 per cent confidence interval. We note that the slight asymmetries of the posteriors imply that the most likely (best-fitting) and median value are very slightly different.

intrinsic thickness along any line of sight, and potentially the gas optical depth, all of which lessen the accuracy of a dynamical model. The molecular gas disc in NGC 7052 is reasonably highly inclined ($i \approx 70^\circ$) and has very small inclination uncertainties which make only a very small contribution to the total $M_{\rm BH}$ uncertainty budget. Indeed, simulations suggest that $i \approx 70^\circ$ appears to be an optimal inclination for accurately recovering SMBH masses from molecular gas kinematics (Davis 2014).

Inaccuracies in the mass model adopted can, in general, also bias the recovered SMBH mass, as an incorrect share of the dynamical mass is assigned to the SMBH. Beside the SMBH, our mass model includes only a contribution from the stellar mass distribution, and it

Downloaded from https://academic.oup.com/mnras/article/503/4/5984/6177668 by Cardiff University user on 22 July 2021

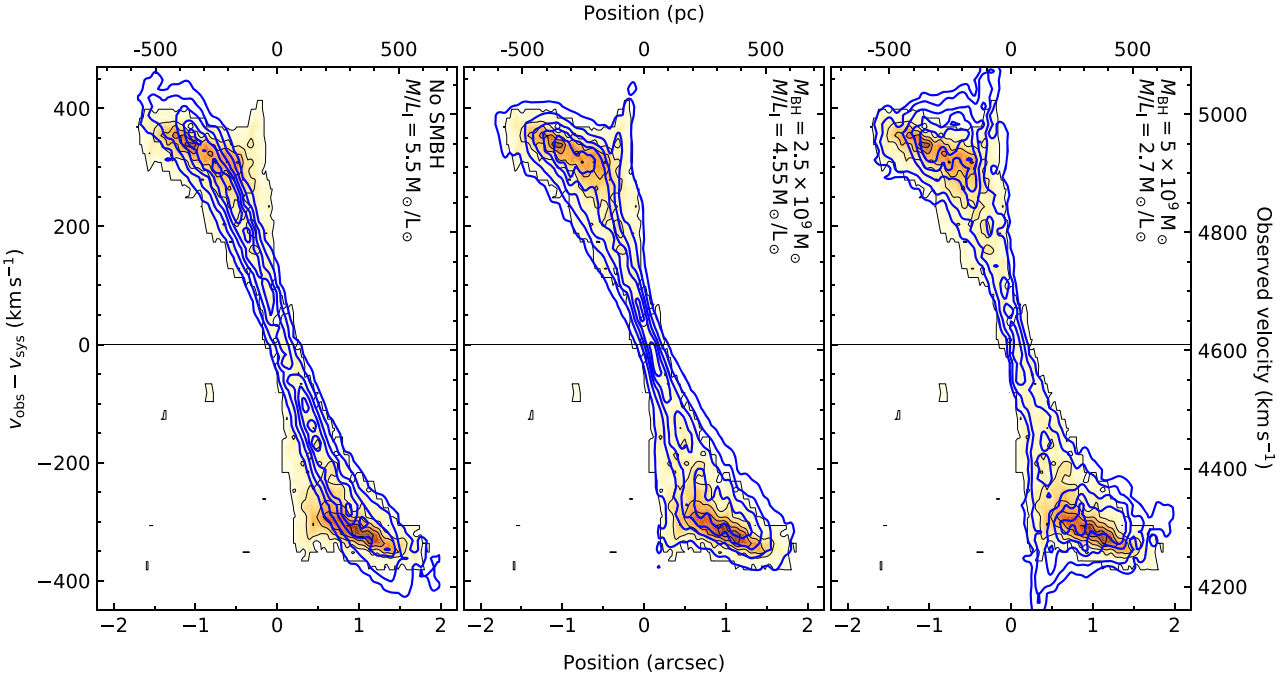

Figure 5. Model position–velocity diagrams along the kinematic major axis of NGC 7052 (blue contours), showing a model without an SMBH (left), with the best-fitting SMBH (centre) and with an overly large SMBH (right). These are overlaid on the observed PVD (orange scales and black contours). The line-of-sight velocities at small radii are enhanced compared to those of a stellar mass-only model, thus requiring additional central mass to fully account for them.

neglects both gas and (dark) halo contributions. However, the relevant length-scale on which these contributions matter is that traced by the CO disc, that extends only to a radius of ≈1.″5. Over such a small-scale dark matter likely makes a negligible contribution to the overall mass budget. Contributions from warm gas ($10^{3.6}$ M$_\odot$ in total; Pandya et al. 2017) and the dust disc (10^4 M$_\odot$ in total; Nieto et al. 1990) are similarly negligible. Naturally, if any of these components were radially distributed identically to the stellar mass, their only effect would in any case be to change the derived dynamical mass-to-light ratio. A radially varying distribution would lead to a mass-to-light ratio gradient, but it would require a significantly centrally concentrated mass distribution to substantially affect the derived M_{BH}.

Fig. 6 shows the enclosed mass of our best-fitting model within spheres of increasing galactic radii, with the contributions from the SMBH, stars and molecular gas indicated separately. Also indicated are the radii corresponding to the synthesized beam and R_{SoI}, the latter using our best-fitting M_{BH} and $\sigma_e = 266$ km s^{-1}(Gültekin et al. 2009). As is clearly seen, the SMBH dominates the galactic potential not only within its nominal sphere of influence, but up to ≈0.″6 (≈200 pc). We thus resolve this region radially with approximately six beams. The molecular gas contribution is negligible at all radii.

We note that the radius at which the SMBH and stars have equal contributions (R_{eq}) is around 60 per cent larger than the nominal SMBH sphere of influence. This is not necessarily concerning, as typical early-type galaxies have R_{eq} slightly larger than R_{SoI} (Yoon 2017).

Next, we consider the accuracy of our adopted stellar mass model. Although the MGE model appears to match well the *HST* F814W image over the centre of the galaxy (Fig. 3), this region is strongly affected by dust. Dust attenuation is expected to decrease the observed flux, and hence cause us to attribute too little mass to the stellar contribution, potentially overestimating M_{BH}. We argue that this effect can be safely disregarded here, as it has been carefully mitigated. First, we adopted the *HST* F814W image of the galaxy

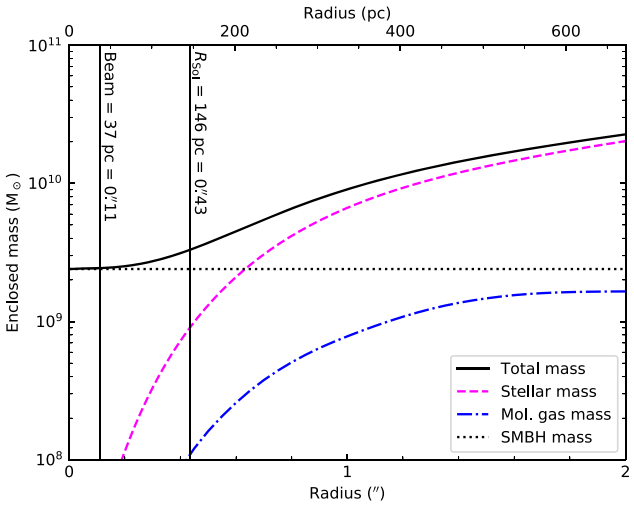

Figure 6. Cumulative mass function of NGC 7052, showing the relative contributions from the SMBH (black dotted line), molecular gas (blue dot-dashed line) and stars (violet dashed line). The total enclosed mass is shown by the solid black line. The physical scales of the synthesized beam and SMBH sphere of influence (assuming our measured SMBH mass and a stellar velocity dispersion $\sigma_e = 266$ km s^{-1}) are indicated by vertical black lines. The molecular gas mass contribution is negligible at all radii.

to build our stellar light model. We also masked the north-western side of the dust disc, where it is in the foreground. Adopting this relatively long wavelength, and masking the foreground dust, will reduce the extinction. Secondly, as we have argued previously, an erroneous stellar light profile can be corrected by an appropriate change to the mass-to-light ratio. Thus, inferring the mass-to-light ratio from beyond the dust disc and assuming it is radially constant

Downloaded from https://academic.oup.com/mnras/article/503/4/5984/6177668 by Cardiff University user on 22 July 2021

would significantly bias our results if no correction was made for dust extinction. However, our stellar mass-to-light ratio is determined purely by the CO kinematics, that only extends across the dust disc. Assuming the extinction due to this disc does not vary dramatically, the effect on the stellar light model will be compensated by an associated change in the mass-to-light ratio. In Section 5.1, we have further shown that there is no evidence for a mass-to-light ratio gradient, that would be a consequence of a substantial deviation of the photometrically derived stellar light profile and the dynamically derived mass profile.

In any case, due to the very high spatial resolution of our data, we probe well into the SMBH-dominated regime, where the stellar contribution is small (see Fig. 6). We therefore conclude that any remaining uncertainties in our stellar light model will not significantly bias our SMBH mass.

We assumed in Section 4 that the CO disc is razor-thin, implemented by setting the z-coordinate (that orthogonal to the disc plane) of the `KinMS` particles to zero. Notionally, a non-negligible disc thickness could account for some of the observed line width along each line of sight, reducing the intrinsic gas velocity dispersion required. To test this assumption, we run another MCMC chain instead giving each particle a z-position drawn from a uniformly distributed radially constant disc thickness of $\pm d$, where d is an additional free model parameter. We adopt a uniform prior of $0 < d < 3.3$ kpc (this upper bound far larger than the disc scale). This chain yields a disc thickness consistent with the synthesized beam, with negligible improvement in the associated best-fitting model's log-likelihood. The associated best-fitting SMBH mass and stellar mass-to-light ratio are unchanged. In addition, the best-fitting gas velocity dispersion found by the new model is not smaller than that found assuming a thin disc by a statistically significant factor. We therefore conclude that the thin disc assumption is acceptable when interpreting data at our resolution, though higher-resolution observations may prove otherwise.

Finally, the adopted distance to NGC 7052 sets the scale of our dynamical model. The inferred SMBH mass scales linearly with distance, since $M_{\rm BH} \propto v^2 R \propto D$, where v is the rotation velocity of a particle at radius R (as we observe an angular radius, the physical radius scales with the assumed distance).

We have adopted a distance of 69.3 Mpc for consistency with the MASSIVE survey (Ma et al. 2014). Although Ma et al. (2014) do not quantify the uncertainty of this distance, the Hubble flow distances listed in the NASA/IPAC Extragalactic Database[5] have a typical uncertainty of 7 per cent. As is standard practice, we do not include this uncertainty in our quoted dynamical SMBH mass measurement, and the results herein can simply be corrected to any adopted distance.

5.3 Gas velocity dispersion

The line-of-sight velocity dispersions observed in molecular gas are comprised of an intrinsic (turbulent) velocity dispersion, broadened by beam smearing of mean velocity gradients. Typical molecular gas intrinsic velocity dispersions are very small (often <10 km s^{-1}; e.g. Davis et al. 2017, 2018; Smith et al. 2019).

van der Marel & van den Bosch (1998) found that the Hα velocity dispersion of NGC 7052 decreased with increasing radius, with a central peak of 400 km s^{-1} falling to 70 km s^{-1} by a radius of $\approx$1 arcsec. Although enhanced central dispersions are expected by Doppler broadening close to the central SMBH, a model excluding an intrinsic velocity dispersion gradient was inconsistent with their observations (van den Bosch & van der Marel 1995). In their dynamical models, they found that an exponentially decaying intrinsic (turbulent) velocity dispersion was required to account for the above variation, of the form

$$\sigma(R) = \sigma_0 + \sigma_1 e^{-R/R_{\rm t}}\,, \tag{2}$$

where $R_{\rm t}$ is the scale length of the (turbulent) velocity dispersion and σ_0 and σ_1 parametrize the radial variation. Their best-fitting dynamical model yielded $\sigma_0 = 60$ km s^{-1}, $\sigma_1 = 523$ km s^{-1} and $R_{\rm t} = 0\farcs11$. The very small scale length implies that although the central amplitude is large, the dispersion is dominated at almost all radii by the (rather large) constant term.

Our best-fitting model described in Section 4 assumed a radially constant velocity dispersion. For comparison, we performed another fit allowing the velocity dispersion to vary with radius according to equation (2). This model is visibly inferior to that found assuming a constant dispersion, but the best-fitting SMBH mass is consistent with our previous result. We therefore conclude that no intrinsic velocity dispersion gradient is required to account for our observations, and our derived SMBH mass is robust.

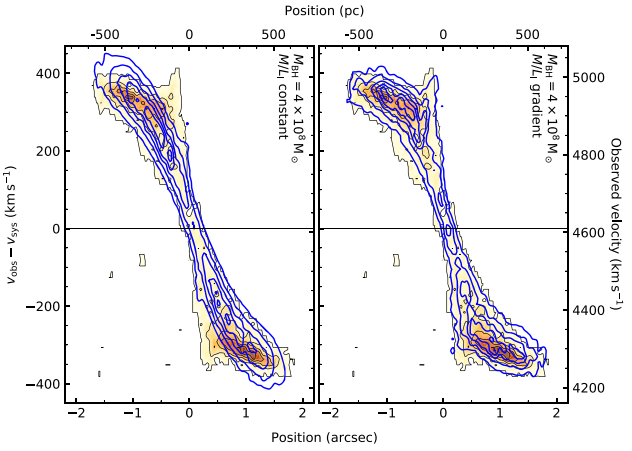

Figure 7. Model position–velocity diagrams along the kinematic major axis of the galaxy (blue contours), showing the best-fitting models with the SMBH mass fixed to that of van der Marel & van den Bosch (1998), with either a radially constant mass-to-light ratio (left), or a mass-to-light ratio gradient (right). These are overlaid on the observed PVD (orange scales and contours). Although allowing a mass-to-light ratio gradient helps to enhance gas velocities at small radii, this model remains inferior to that described in Section 4.4.

5.4 Comparison with ionized gas

van der Marel & van den Bosch (1998) used Hα and [N II] emission observed with the *HST* Faint Object Spectrograph to measure the central SMBH mass of NGC 7052, and found $M_{\rm BH} = 3.9^{+2.7}_{-1.5} \times 10^8$ M$_\odot$ (corrected to our adopted distance). Our measurement is not consistent with this result.

As a check, we performed another fit to our observations, with the SMBH mass set to that found by van der Marel & van den Bosch (1998) from warm gas kinematics. The major-axis PVD of the model with the maximum log-likelihood is shown in Fig. 7 (left panel), overlaid on our ALMA data. Clearly, the model severely underestimates the molecular gas velocities at small radii, as would be expected from imposing an SMBH mass one-quarter of that required.

[5] http://ned.ipac.caltech.edu

Downloaded from https://academic.oup.com/mnras/article/503/4/5984/6177668 by Cardiff University user on 22 July 2021

This can be partially compensated for by allowing a stellar mass-to-light ratio gradient. We thus include a gradient in yet another model by calculating the circular velocity as before, but assuming $M/L_{\rm I} = 1\,{\rm M}_{\odot}/{\rm L}_{\odot,{\rm I}}$, and then multiplying this function at each radius by $\sqrt{M/L_{\rm I}(R)}$ (Davis & McDermid 2017; Davis et al. 2018). We adopt a linearly varying mass-to-light ratio that flattens beyond 2 arcsec. The best-fitting model is shown in Fig. 7 (right-hand panel), and has a central mass-to-light ratio of $6.9\,{\rm M}_{\odot}/{\rm L}_{\odot,{\rm I}}$, returning to $4.6\,{\rm M}_{\odot}/{\rm L}_{\odot,{\rm I}}$ (our best-fitting spatially constant M/L_I) at 2 arcsec. Although as expected the M/L gradient increases the central velocities, the model is still inferior to that presented in Section 5.1. As we discussed in Section 5.2, a discrete increase in the mass-to-light ratio at very small (spatially unresolved) scales can always mimic an SMBH signature, but there is no physical reason to expect such a change. We therefore conclude here that such a mass-to-light ratio gradient is disfavoured, and hence that the $M_{\rm BH}$ measurement of van der Marel & van den Bosch (1998) is excluded by our data.

The main advantages of our molecular gas observations over those used by van der Marel & van den Bosch (1998) are as follows. First, our observations trace the entire gas disc, rather than only a few discrete locations along the major axis (the galactic radii of which can themselves have significant uncertainty due to pointing uncertainty). By fitting the entire gas disc, we have many more constraints on the observed kinematics (and the uncertainty on their locations), and hence on the mass distribution throughout the central region of the galaxy. Second, all gas dynamical measurements can be affected by non-gravitational forces and non-circular motions. The very low velocity dispersions of our CO gas indicate that these are negligible (while warm ionized gas is likely to be more significantly affected). As outlined in Section 5.3, van der Marel & van den Bosch (1998) required a significant central velocity dispersion to adequately fit their observations, attributed to turbulence and neglected in the dynamical model. If this dispersion instead corresponds to (some component of) pressure support, the fit will necessarily underestimate the SMBH mass. It should be further noted that more recent *HST* Space Telescope Imaging Spectrograph observations indicate the presence of a separate ionized-gas dynamical component (perhaps a broad-line region; Noel-Storr et al. 2003; Verdoes Kleijn, van der Marel & Noel-Storr 2006; Noel-Storr, Baum & O'Dea 2007), which may exhibit significantly different kinematics to that of the extended gas detected by the FOS.

A similar case of a rotating warm gas disc with a strong velocity dispersion gradient is found in Centaurus A. Häring-Neumayer et al. (2006) explored the sensitivity of SMBH masses inferred from dynamical models to the inclusion of the velocity dispersion gradient as component of the dynamical support. They found that a cold disc assumption could underestimate the SMBH mass by a factor of $\approx$3 in their case, with respect to a model including the velocity dispersion gradient. Although the degree to which the lack of this support can underestimate the SMBH mass will vary between discs, this evidence suggests that the lack of dynamical pressure support in the warm gas model of van der Marel & van den Bosch (1998) could be the reason for the disagreement between their inferred SMBH mass and ours.

The $M_{\rm BH}$–$\sigma_{\rm e}$ relation of Sahu, Graham & Davis (2019) predicts $M_{\rm BH} = 1.0^{+2.1}_{-0.7} \times 10^9\,{\rm M}_{\odot}$ for NGC 7052 (assuming $\sigma_{\rm e} = 266 \pm 13\,{\rm km\ s^{-1}}$, and including 0.44 dex of intrinsic scatter). Our result is in excellent agreement with this prediction, whereas the ionized-gas measurement of van der Marel & van den Bosch (1998) is significantly below it. The significant differences across SMBH masses derived via different dynamical tracers thus continues to demonstrate the need for robust cross-checks between all techniques. Further SMBH mass measurements using molecular gas offer the prospect of determining the intrinsic scatters of the SMBH-host galaxy scaling relations with measurements from a single technique across the entire Hubble sequence.

5.5 Tidal accelerations and molecular cloud stability in the galactic centre

The molecular gas discs of many galaxies in the WISDOM sample exhibit central holes at small radii (e.g. Davis et al. 2018; Smith et al. 2019), including NGC 7052. These $\approx$100 pc holes have been revealed for the first time by the exceptionally high angular resolutions required for SMBH measurements. The typical extents of these features are roughly consistent with the SMBH spheres-of-influence, suggesting that they may have a dynamical origin.

One dynamical mechanism that could give rise to depleted molecular gas surface densities at the centre of galaxies is the tidal disruption of gas clouds. It is generally believed that molecular gas forms in these clouds, due to the outer layers of the clouds shielding their centres from ultraviolet radiation that would otherwise photo-dissociate the molecules, and due to the high densities increasing the number of collisions that can form molecules (and those with dust grains that can enhance molecule formation through surface reactions; Binney & Merrifield 1998). Strong shear or tidal acceleration could exceed the self-gravity of such clouds, disrupting them and exposing the molecules to photodissociation, or preventing the formation of clouds entirely. This would in turn inhibit the formation of stars near an SMBH (e.g. Sarzi et al. 2005).

Liu et al. (2021) considered the effect of external gravity on the morphology and confinement of giant molecular clouds. In their formalism, spatial variations of the external gravitational potential can contribute to either keeping clouds bound or to disrupting them, depending on the sign of $T - 2\Omega^2$, where

$$T(R) \equiv -R \left. \frac{{\rm d}\Omega^2(r)}{{\rm d}r} \right|_R \tag{3}$$

is the tidal acceleration in the radial direction and Ω is the orbital angular velocity (v/R; see appendix A of Liu et al. 2021). These quantities, derived from our best-fitting dynamical model, are shown in the bottom panel of Fig. 8. Uncertainties in each are estimated by propagating the uncertainties in our model parameters via Monte Carlo methods.

Our model indicates that $T - 2\Omega^2$ changes sign at $0\farcs50 \pm 0\farcs09$ and is positive (thus disrupting the clouds) within this radius. This position is consistent with the peak of the gas distribution (Fig. 8, top panel). If other contributions to the energy budgets of clouds at these radii are negligible (or, more likely, are finely balanced by gravity), the central gas deficit could be the result of tidal accelerations disrupting the clouds. We cannot directly measure these other contributions in NGC 7052, and thus cannot robustly test this hypothesis.

Entirely different explanations are of course also possible. Emission from a central AGN could contribute sufficient photons to dissociate the CO molecules. Alternatively, holes may be better traced by higher-J CO transitions (e.g. García-Burillo et al. 2016), or by dense molecular gas emission (e.g. Imanishi et al. 2018). The holes found thus far by the WISDOM project (Davis et al. 2018; Smith et al. 2019 and this work, plus a slight central depression in North et al. 2019) do not appear to be correlated with AGN activity. Another dynamical possibility is that resonances due to non-axisymmetric features in the potential could cause the central hole. Davis et al. (2018) investigated this for NGC 4429 and concluded

Downloaded from https://academic.oup.com/mnras/article/503/4/5984/6177668 by Cardiff University user on 22 July 2021

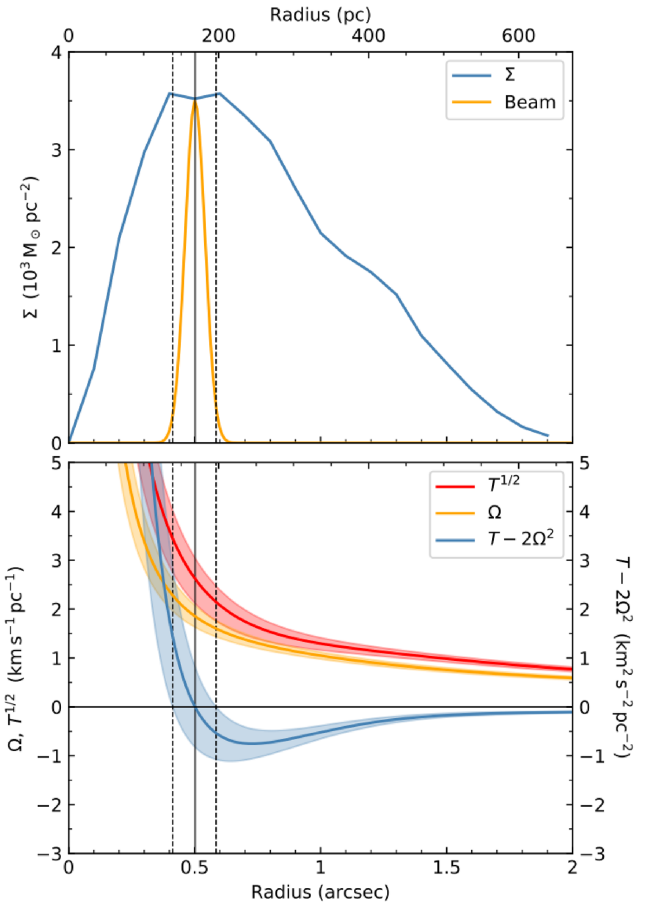

Figure 8. Top panel: Azimuthally averaged molecular gas surface density radial profile (Σ; blue solid line), overlaid with our synthesized beam (orange solid line) centred at 0.″5. Bottom panel: Orbital angular velocity (Ω, orange solid line), tidal acceleration per unit length in the radial direction (T, red solid line), and the function $T - 2\Omega^2$ (blue solid line), all calculated from our best-fitting dynamical model. Coloured envelopes around each line indicate the $\pm 3\sigma$ confidence intervals. $T - 2\Omega^2$ is positive within $0.''50 \pm 0.''09$, indicated by a black vertical line (with 3σ confidence intervals indicated by black dashed vertical lines) in both panels. This matches well the maximum of the surface density profile, and thus the radius within which the molecular gas density rapidly decreases.

that an unusually fast pattern speed would be required, making this explanation unlikely.

6 CONCLUSIONS

High angular resolution observations from the ALMA and Atacama Compact Array (ACA) were used to make a 1.3 mm continuum image and a ^{12}CO(2-1) cube of the elliptical galaxy NGC 7052. We detect a compact continuum source at the optical centre of the galaxy, assumed to correspond to emission from the active galactic nucleus. The CO data reveal a dynamically cold ($\sigma \approx 20$ km s^{-1}) rotating disc coincident with a prominent dust disc visible in *HST* images. The ALMA observations resolve a physical scale of 0.″11 (37 pc), smaller than the central region over which the galactic gravitational potential is dominated by the central SMBH.

We constructed a dynamical model of NGC 7052 to constrain the SMBH mass. We estimated the stellar contribution to the potential by multiplying a multi-Gaussian expansion of a *HST* WFPC2/PC F814W optical image by a spatially constant mass-to-light ratio. The model was fit to the central $2.''56 \times 2.''56$ region of the ALMA data cube within an MCMC framework. The inferred SMBH mass is $(2.5 \pm 0.3) \times 10^9$ M$_\odot$ and the I-band mass-to-light ratio is (4.6 ± 0.2) M$_\odot$/L$_{\odot,\mathrm{I}}$ (3σ confidence intervals). We exclude the possibility of a physically motivated mass-to-light ratio gradient.

This SMBH mass measurement is substantially larger than that found previously using *HST* Faint Object Spectrograph observations of ionized gas by van der Marel & van den Bosch (1998). The key difference is that the molecular gas disc is dynamically cold even very close to the SMBH, whereas the warm gas kinematics of van der Marel & van den Bosch (1998) show large velocity dispersion gradients. Our observations strongly exclude their previous measurement. We suggest that our larger SMBH mass measurement is due to the fact that they did not include dynamical pressure support in their models.

The peak molecular gas surface density occurs at a radius of $\approx 0.''5$, the surface density slowly declining towards the centre of the galaxy (and outward). This peak corresponds to the radius within which the external gravitational potential acts to tidally disrupt molecular gas clouds. We suggest that if this effect dominates the self-gravity of clouds, it is likely that the central molecular gas depletion is the result of tidal forces preventing the formation of molecular clouds.

Our SMBH measurement once more demonstrates the power of the molecular gas kinematics method to accurately measure SMBH masses, and the important role ALMA can play to understand the dynamics of molecular gas in the central regions of galaxies. The steadily increasing sample of such masses will soon allow us to constrain the M_{BH}–σ_{e} relation over several orders of magnitude in SMBH mass with a single method.

ACKNOWLEDGEMENTS

MDS acknowledges support from a Science and Technology Facilities Council (STFC) DPhil studentship under grant ST/N504233/1. MB was supported by STFC consolidated grant 'Astrophysics at Oxford' ST/H002456/1 and ST/K00106X/1. TAD was supported by STFC consolidated grant ST/S00033X/1. MC acknowledges support from a Royal Society University Research Fellowship. TGW acknowledges funding from the European Research Council (ERC) under the European Union's Horizon 2020 Framework Programme (grant agreement No. 694343).

This paper makes use of the following ALMA data: ADS/JAO.ALMA #2016.2.00046.S and #2018.1.00397.S. ALMA is a partnership of ESO (representing its member states), NSF (USA), and NINS (Japan), together with NRC (Canada), MOST and ASIAA (Taiwan), and KASI (Republic of Korea), in cooperation with the Republic of Chile. The Joint ALMA Observatory is operated by ESO, AUI/NRAO, and NAOJ.

This research has made use of the NASA/IPAC Extragalactic Database (NED), which is operated by the Jet Propulsion Laboratory, California Institute of Technology, under contract with the National Aeronautics and Space Administration. This paper has also made use of the HyperLeda data base (http://leda.univ-lyon1.fr).

DATA AVAILABILITY

The observations underlying this article are available in the ALMA archive, at https://almascience.eso.org/asax/, and in the Hubble Legacy Archive, at https://hla.stsci.edu.

Downloaded from https://academic.oup.com/mnras/article/503/4/5984/6177668 by Cardiff University user on 22 July 2021

REFERENCES

Barth A. J., Boizelle B. D., Darling J., Baker A. J., Buote D. A., Ho L. C., Walsh J. L., 2016a, ApJ, 822, L28
Barth A. J., Darling J., Baker A. J., Boizelle B. D., Buote D. A., Ho L. C., Walsh J. L., 2016b, ApJ, 823, 51
Beifiori A., Courteau S., Corsini E. M., Zhu Y., 2012, MNRAS, 419, 2497
Benson A. J., Bower R. G., Frenk C. S., Lacey C. G., Baugh C. M., Cole S., 2003, ApJ, 599, 38
Binney J., Merrifield M., 1998, Galactic Astronomy. Princeton Series in Astrophysics. Princeton Univ. Press, Princeton, New Jersey, USA
Boizelle B. D., Barth A. J., Walsh J. L., Buote D. A., Baker A. J., Darling J., Ho L. C., 2019, ApJ, 881, 10
Bolatto A. D., Wolfire M., Leroy A. K., 2013, ARA&A, 51, 207
Braatz J. A., Wilson A. S., Henkel C., 1996, ApJS, 106, 51
Capetti A., Celotti A., 1999, MNRAS, 304, 434
Capetti A., Trussoni E., Celotti A., Feretti L., Chiaberge M., 2000, MNRAS, 318, 493
Capetti A., Celotti A., Chiaberge M., de Ruiter H. R., Fanti R., Morganti R., Parma P., 2002, A&A, 383, 104
Cappellari M., 2002, MNRAS, 333, 400
Cappellari M., Verolme E. K., van der Marel R. P., Verdoes Kleijn G. A., Illingworth G. D., Franx M., Carollo C. M., de Zeeuw P. T., 2002, ApJ, 578, 787
Condon J. J., Frayer D. T., Broderick J. J., 1991, AJ, 101, 362
Dame T. M., 2011, preprint (arXiv:1101.1499)
Davis T. A., 2014, MNRAS, 443, 911
Davis T. A., McDermid R. M., 2017, MNRAS, 464, 453
Davis T. A. et al., 2013a, MNRAS, 429, 534
Davis T. A., Bureau M., Cappellari M., Sarzi M., Blitz L., 2013b, Nature, 494, 328
Davis T. A., Bureau M., Onishi K., Cappellari M., Iguchi S., Sarzi M., 2017, MNRAS, 468, 4675
Davis T. A. et al., 2018, MNRAS, 473, 3818
Davis T. A. et al., 2020, MNRAS, 496, 4061
Di Matteo T., Springel V., Hernquist L., 2005, Nature, 433, 604
Donato D., Sambruna R. M., Gliozzi M., 2004, ApJ, 617, 915
Emsellem E., Monnet G., Bacon R., 1994, A&A, 285, 723
Emsellem E. et al., 2011, MNRAS, 414, 888
Fanti C., Fanti R., Gioia I. M., Lari C., Parma P., Ulrich M. H., 1977, A&AS, 29, 279
Ferrarese L., Merritt D., 2000, ApJ, 539, L9
Gao F. et al., 2017, ApJ, 834, 52
García-Burillo S. et al., 2016, ApJ, 823, L12
Gebhardt K. et al., 2000, ApJ, 539, L13
Goulding A. D. et al., 2016, ApJ, 826, 167
Graham A. W., Erwin P., Caon N., Trujillo I., 2001, ApJ, 563, L11
Greenhill L. J., Henkel C., Becker R., Wilson T. L., Wouterloot J. G. A., 1995, A&A, 304, 21
Gültekin K. et al., 2009, ApJ, 698, 198
Häring-Neumayer N., Cappellari M., Rix H. W., Hartung M., Prieto M. A., Meisenheimer K., Lenzen R., 2006, ApJ, 643, 226
Hernquist L., 1989, Nature, 340, 687
Holtzman J. A., Burrows C. J., Casertano S., Hester J. J., Trauger J. T., Watson A. M., Worthey G., 1995, PASP, 107, 1065
Imanishi M., Nakanishi K., Izumi T., Wada K., 2018, ApJ, 853, L25
Kormendy J., Gebhardt K., 2001, in Wheeler J. C., Martel H., eds, AIP Conf. Proc. Vol. 586, 20th Texas Symposium on Relativistic Astrophysics. Am. Inst. Phys., New York, p. 363
Kormendy J., Ho L. C., 2013, ARA&A, 51, 511
Kormendy J., Richstone D., 1995, ARA&A, 33, 581
Krajnović D., Cappellari M., McDermid R. M., 2018, MNRAS, 473, 5237
Kuo C. Y. et al., 2011, ApJ, 727, 20
Liu L. et al., 2021, MNRAS, in revision
Ma C.-P., Greene J. E., McConnell N., Janish R., Blakeslee J. P., Thomas J., Murphy J. D., 2014, ApJ, 795, 158
McMullin J. P., Waters B., Schiebel D., Young W., Golap K., 2007, in Shaw R. A., Hill F., Bell D. J., eds, ASP Conf. Ser. Vol. 376, Astronomical Data Analysis Software and Systems XVI. Astron. Soc. Pac., San Francisco, p. 127
McNamara B. R., Nulsen P. E. J., 2007, ARA&A, 45, 117
Magorrian J. et al., 1998, AJ, 115, 2285
Memola E., Trinchieri G., Wolter A., Focardi P., Kelm B., 2009, A&A, 497, 359
Mitzkus M., Cappellari M., Walcher C. J., 2017, MNRAS, 464, 4789
Miyoshi M., Moran J., Herrnstein J., Greenhill L., Nakai N., Diamond P., Inoue M., 1995, Nature, 373, 127
Mould J. R. et al., 2000, ApJ, 529, 786
Mulchaey J. S., Jeltema T. E., 2010, ApJ, 715, L1
Nagai H. et al., 2019, ApJ, 883, 193
Nguyen D. D. et al., 2020, ApJ, 892, 68
Nieto J. L., McClure R., Fletcher J. M., Arnaud J., Bacon R., Bender R., Comte G., Poulain P., 1990, A&A, 235, L17
Noel-Storr J., Baum S. A., Verdoes Kleijn G., van der Marel R. P., O'Dea C. P., de Zeeuw P. T., Carollo C. M., 2003, ApJS, 148, 419
Noel-Storr J., Baum S. A., O'Dea C. P., 2007, ApJ, 663, 71
North E. V. et al., 2019, MNRAS, 490, 319
Onishi K., Iguchi S., Davis T. A., Bureau M., Cappellari M., Sarzi M., Blitz L., 2017, MNRAS, 468, 4663
Pandya V. et al., 2017, ApJ, 837, 40
Parma P., de Ruiter H. R., Fanti C., Fanti R., 1986, A&AS, 64, 135
Saglia R. P. et al., 2016, ApJ, 818, 47
Sahu N., Graham A. W., Davis B. L., 2019, ApJ, 887, 10
Sanders D. B., Soifer B. T., Elias J. H., Madore B. F., Matthews K., Neugebauer G., Scoville N. Z., 1988, ApJ, 325, 74
Sarzi M., Rix H.-W., Shields J. C., Ho L. C., Barth A. J., Rudnick G., Filippenko A. V., Sargent W. L. W., 2005, ApJ, 628, 169
Simmons B. D., Smethurst R. J., Lintott C., 2017, MNRAS, 470, 1559
Smith M. D. et al., 2019, MNRAS, 485, 4359
Smith M. D. et al., 2021, MNRAS, 500, 1933
Thater S., Krajnović D., Nguyen D. D., Iguchi S., Weilbacher P. M., 2020, in Valluri M., Sellwood J. A., eds, IAU Symp. Vol. 353, Galactic Dynamics in the Era of Large Surveys. Kluwer, Dordrecht, p. 199
van den Bosch F. C., van der Marel R. P., 1995, MNRAS, 274, 884
van den Bosch R. C. E., 2016, ApJ, 831, 134
van den Bosch R. C. E., van de Ven G., 2009, MNRAS, 398, 1117
van der Marel R. P., van den Bosch F. C., 1998, AJ, 116, 2220
Veale M., Ma C.-P., Greene J. E., Thomas J., Blakeslee J. P., McConnell N., Walsh J. L., Ito J., 2017, MNRAS, 471, 1428
Verdoes Kleijn G. A., van der Marel R. P., Noel-Storr J., 2006, AJ, 131, 1961
Wang Z., Kenney J. D. P., Ishizuki S., 1992, AJ, 104, 2097
Willmer C. N. A., 2018, ApJS, 236, 47
Yoon I., 2017, MNRAS, 466, 1987

This paper has been typeset from a TEX/LATEX file prepared by the author.

Downloaded from https://academic.oup.com/mnras/article/503/4/5984/6177668 by Cardiff University user on 22 July 2021